

Optimized Viewing Angles for Cardiac Electrophysiology Ablation Procedures

Martin Koch · Matthias Hoffmann · Marcus Pfister ·
Joachim Hornegger · Norbert Strobel

Received: date / Accepted: date

Abstract

Purpose

Catheter ablation is a common treatment option for atrial fibrillation (AF). Interventional C-arm X-ray systems are used for guiding AF procedures, employing standard view positions. Since the projection angles are not adapted to the individual patient anatomy, standard projections do not necessarily offer the best views of important anatomical structures. Using a pre-procedural 3-D data set acquired with MRI or CT, suitable ablation sites (lines) can be identified in advance so an ablation plan can be superimposed on fluoroscopic images to guide the procedure.

Methods

A method was developed to estimate optimized projection views for biplane X-ray C-arm systems based on planning data for AF ablation procedures. The estimated viewing angles were compared to standard angulations using an objective quality metric, the length of the planned ablation line as seen under X-ray. This method was tested using 35 clinical datasets annotated with planned ablation lines for ipsilateral pulmonary vein isolation.

Results

M. Koch · M. Hoffmann · J. Hornegger
Pattern Recognition Lab, Friedrich-Alexander-Universität
Erlangen-Nürnberg, Martensstr. 3, 91058 Erlangen, Germany,
E-mail: Martin.Koch@cs.fau.de

J. Hornegger
Erlangen Graduate School in Advanced Optical Technologies (SAOT), Friedrich-Alexander-Universität Erlangen-Nürnberg, Paul-Gordan-Str. 6, 91058 Erlangen, Germany

M. Pfister · N. Strobel
Siemens AG, Healthcare Sector, Siemensstr. 1, 91301 Forchheim, Germany

The optimized views computed using the new method yielded 28 % less foreshortening of pre-planned ablation lines on average. In one case, anatomy-based view calculation lead to a 69 % reduction in foreshortening.

Conclusion

The commonly used standard views provide reasonable a priori choices and some improvement is possible by switching among common angulations depending on the treatment region. Further gains are possible by using anatomy-optimized biplane C-arm angulations.

Keywords Electrophysiology, Fluoroscopic projection, Pulmonary vein isolation, Treatment planning

1 Introduction

Radiofrequency catheter ablation is a common method for the treatment for heart arrhythmias [18]. These procedures involve a C-arm fluoroscopy system. Currently, procedures are usually performed using standard C-arm angulations. Common angulations are anterior-posterior (AP), 30°–45° right anterior oblique (RAO), and 45°–60° left anterior oblique (LAO). For electrophysiology ablation procedures, the C-arms are usually not angled toward the head or the feet, i.e., in cranial (CRAN) or caudal (CAUD) orientation. Commonly used combinations of viewing angles for biplane C-arm systems are shown in Table 1. The C-arm view angles α_A and β_A refer to primary and secondary angle of the A-plane, respectively. The view orientations α_B and β_B define the corresponding rotations of the B-plane. Typical C-arm view angles α_A for monoplane C-arm systems are 30° RAO, 60° LAO, 45° RAO, 45° LAO or AP direction.

In the remainder of the paper, we focus on atrial fibrillation, the most common heart arrhythmia. The

Table 1 Commonly used angulations for biplane C-arm X-ray systems during AF ablation procedures.

| | α_A | β_A | α_B | β_B |
|------|------------|-----------|------------|-----------|
| Std1 | 30° RAO | 0° CRAN | 60° LAO | 0° CRAN |
| Std2 | 45° RAO | 0° CRAN | 45° LAO | 0° CRAN |
| Std3 | 0° RAO | 0° CRAN | 90° LAO | 0° CRAN |

main goal during ablative treatment for atrial fibrillation is the isolation of the pulmonary veins (PVs) [9]. In this context, Tang et al. investigated the orientation of pulmonary vein ostia in atrial fibrillation patients as seen under X-ray. During their study of optimal fluoroscopic projections for pulmonary vein angiographies, they found that there is a different optimal projection angle for every pulmonary vein ostium [17].

For atrial fibrillation, automatic planning methods have been proposed [11,13]. Based on a particular patient anatomy, e.g. extracted from pre-procedural 3-D imaging, such as CT or MRI, appropriate ablation lines can be computed. They may be superimposed on X-ray images during the procedure to obtain additional information for catheter navigation [4,1]. We can use these planned ablation lines, usually placed around the ipsilateral pulmonary veins, to optimize C-arm projection angles. Taking into account the actual treatment plan when setting up the X-ray view directions may provide the physician with valuable insights which he may miss out on otherwise.

Estimation of optimal views for interventional X-ray systems has been investigated widely for coronary angiography [3,5,6,7,12]. The work by Dumay et al. and Chen et al. is particularly relevant for our approach, because both used foreshortening as an optimization criterion. They modeled coronaries as vectors. Optimality was defined as minimal foreshortening of a selected vessel structure of interest. This is achieved in so-called triple optimal views. Here, the vessel segment is parallel to both imaging planes, and the two C-arm views are orthogonal to each other. For objects that can be described by a vector, triple optimal views can be obtained for a variety of angle combinations. In [5], the user may choose one rotation angle freely. Then, the remaining angles are calculated to satisfy the optimality constraints. Chen et al. proposed an objective function to measure the foreshortening of vessel segments [3]. Besides vessel foreshortening, vessel overlap is also evaluated with focus on bifurcations of the coronary tree.

In this paper, we propose a new method to estimate optimal viewing directions. Unlike in [5] and [3], who considered (1-D) vessel segments, we are estimating optimal views on 2-D structures such as ellipses or planes. Our method allows for different optimality criteria depending on physicians' preferences or use cases.

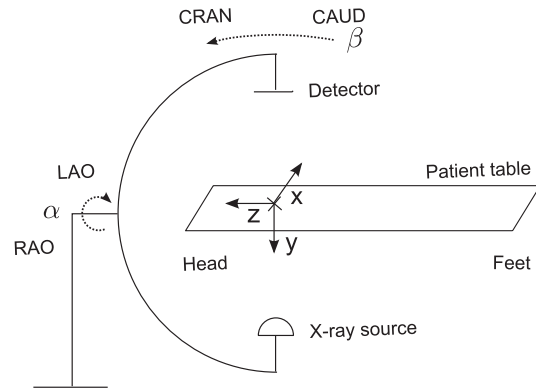


Fig. 1 Schematic drawing of an interventional C-arm mono-plane X-ray system. The dashed arrows α and β depict the primary and secondary rotation angle of the C-arm. LAO and RAO are labels for primary angle rotations: left-/ right- anterior oblique. CRAN and CAUD describe rotations around the secondary angle, toward the patient's head or feet, respectively. The origin of the world coordinate system coincides with the isocenter of the X-ray system.

We evaluated our approach in terms of overall optimality, as well as constrained optimality due to mechanical system limitations. Depending on how an X-ray device is built, not all viewing directions are achievable. The quality metric applied is based on best visibility of ablation target sites characterized by minimal foreshortening. Our approach was evaluated on 35 clinical datasets of atrial fibrillation procedures augmented with professionally planned ablation lines.

2 Materials and Methods

Interventional C-arm X-ray systems can rotate the X-ray tube and detector to obtain different viewing angles during an interventional procedure. A schematic drawing of a single C-arm explaining the primary and secondary rotation angles α and β is presented in Figure 1. The system is shown in the initial position, with both rotation angles equal to zero. In case of a biplane C-arm system, the initial position of the second plane (B-plane) is at $\alpha = 90^\circ$. Typical angulations for a biplane system during atrial fibrillation ablation procedures are listed in Table 1. Note that positive view angles for the primary angle, α , are associated with left anterior (LAO) views. Negative view angles, on the other hand, describe projections taken from a right anterior (RAO) view position. Positive/negative angles for the secondary angle, β , denote cranial/caudal views, respectively. A common goal when taking projection images is to position the X-ray system such that it acquires views representing the anatomy of interest as accurately as possible, i.e., with minimal foreshortening.

In the case of pulmonary vein isolation, the areas of interest are the (ipsilateral) pulmonary vein ostia. For enhanced navigation during the ablation procedure, desirable ablation lines can be added to a graphical representation (model) of the patient's left atrium. The resulting graphical scene can then be fused with live X-ray images [1]. Each ablation line approximately forms an ellipse. To see the treatment region with minimal foreshortening, the imaging system has to be positioned such that a frontal (straight) view onto the ablation line can be obtained. To optimize view directions, the 2-D structure, in our case an ellipse, is approximated as a plane. In an ideal case, the angle between the viewing direction, represented by the X-ray central beam, and the plane normal vector should either be 0° for a frontal view or 90° for a sagittal view onto the object, respectively. With real systems, we can try to approach these conditions, but there are limitations as further explained below.

2.1 Plane Fitting

For actual patient data, planned ablation lines are unlikely to lie completely within a plane. To estimate a plane that best fits the corresponding planning data, the ablation line is equidistantly sampled. Sample points are labeled \mathbf{x}_i , with $i = 0 \dots N$. The plane is estimated to minimize the squared distance of the sample points \mathbf{x}_i . To compute the plane normal vector \mathbf{n} , first the eigenvectors of the point cloud described by the sample points are calculated using singular value decomposition. The cross product of the eigenvectors \mathbf{e}_1 , \mathbf{e}_2 , corresponding to the two main eigenvalues, produces the orthogonal vector \mathbf{n} .

$$\mathbf{n} = \mathbf{e}_1 \times \mathbf{e}_2 \quad (1)$$

The normal vector is oriented such that it directs away from the antrum toward the pulmonary veins. Since the plane estimation can be applied to any point clouds around a plane-like structure, it is easy to apply our method to use cases beyond atrial fibrillation.

2.2 Optimal Viewing Direction

The optimal viewing direction is defined by a normal vector in 3-D space. The normal vector $\mathbf{n} = (n_x, n_y, n_z)$ can easily be transferred into corresponding primary and secondary angles of an unconstrained C-arm sys-

tem via standard trigonometry functions:

$$\alpha = \begin{cases} \arctan\left(\frac{n_x}{-n_y}\right) & \text{if } n_y \neq 0, \\ \frac{\pi}{2} & \text{if } n_x \geq 0, \\ -\frac{\pi}{2} & \text{if } n_x < 0, \end{cases} \quad (2)$$

$$\beta = \arcsin(n_z) \quad (3)$$

A schematic drawing of the C-arm system as well as the corresponding angles can be seen in Figure 1.

To compute the C-arm viewing direction $\mathbf{v}(\alpha, \beta)$ based on the primary and secondary angle, the two rotations R_α and R_β are applied. The rotation matrix for the primary angle rotation is described as

$$R_\alpha = \begin{bmatrix} \cos \alpha & -\sin \alpha & 0 \\ \sin \alpha & \cos \alpha & 0 \\ 0 & 0 & 1 \end{bmatrix} \quad (4)$$

For the secondary angle rotation, the corresponding rotation matrix can be computed based on the Rodrigues formula with the rotation axis $\mathbf{u} = R_\alpha \mathbf{u}_0$. The vector \mathbf{u}_0 is set to $[-1 \ 0 \ 0]^T$, the initial position of the rotation axis. The rotation matrix for the secondary rotation is described as

$$R_\beta = \cos(\beta)I + (1 - \cos(\beta))\mathbf{u}\mathbf{u}^T + \sin(\beta)[\mathbf{u}]_\times, \quad (5)$$

with

$$[\mathbf{u}]_\times = \begin{bmatrix} 0 & -u_z & u_y \\ u_z & 0 & -u_x \\ -u_y & u_x & 0 \end{bmatrix}. \quad (6)$$

The C-arm viewing direction can then be computed as

$$\mathbf{v}(\alpha, \beta) = R_\beta R_\alpha \mathbf{v}_0. \quad (7)$$

If we multiply both matrices R_β and R_α , they simplify due to trigonometric identities, and we obtain:

$$R_{\alpha,\beta} = R_\beta R_\alpha = \begin{bmatrix} \cos(\alpha) & -\sin(\alpha)\cos(\beta) & -\sin(\alpha)\sin(\beta) \\ \sin(\alpha) & \cos(\alpha)\cos(\beta) & \cos(\alpha)\sin(\beta) \\ \sin(\alpha)\sin(\beta)\cos(\alpha) & -\sin(\beta) & \cos(\beta) \end{bmatrix}. \quad (8)$$

Unfortunately, not all angulations can be reached by a conventional C-arm system. Due to mechanical constraints, primary and secondary angles can only vary within a certain range. The domain of possible angulations differs for A-plane and B-plane, respectively. We want to estimate a mechanically feasible angulation of the C-arm that is as close to the optimal view as possible. This similarity is expressed by the scalar product of the plane's normal vector, \mathbf{n} , and the viewing direction of the C-arm system $\mathbf{v}(\alpha, \beta)$. In other words, for optimized frontal/sagittal view directions, we want to maximize/minimize the magnitude of the scalar product within the given mechanical C-arm constraints.

In case of a monoplane C-arm system, only one viewing direction (for the A-plane) has to be optimized.

For a good frontal view onto the planned ablation line, the problem can be formulated as constrained maximization problem:

$$\begin{aligned} & \operatorname{argmax}_{\alpha_A, \beta_A} |\mathbf{v}_A(\alpha_A, \beta_A) \circ \mathbf{n}| \\ & \text{s.t.} \begin{cases} \alpha_{A, \min} \leq \alpha_A \leq \alpha_{A, \max} \\ \beta_{A, \min} \leq \beta_A \leq \beta_{A, \max} \end{cases} \quad (9) \end{aligned}$$

The angles α_A, β_A define the viewing direction $\mathbf{v}_A(\alpha_A, \beta_A)$ of the A-plane, while $\alpha_{A, \min}, \alpha_{A, \max}, \beta_{A, \min}, \beta_{A, \max}$ define the boundaries of the applicable range for each angle separately.

In case of biplane C-arm systems, both viewing directions, for A-plane and B-plane, should be optimized together. In this case, $\mathbf{v}_B(\alpha_B, \beta_B)$ defines the view direction of the B-plane. Similar to the constraints on the A-plane angles, there are mechanical limitations for the B-plane, expressed as $\alpha_{B, \min}, \alpha_{B, \max}, \beta_{B, \min}, \beta_{B, \max}$. They define the range of possible view directions for the B-plane C-arm. Additional constraints have to be taken into account between the two viewing directions of the A-plane C-arm and the B-plane C-arm, respectively. The angle $\gamma_{A, B}$ describes the angle between the two viewing directions \mathbf{v}_A and \mathbf{v}_B . The joint optimization can be formulated as follows:

$$\begin{aligned} & \operatorname{argmax}_{\alpha_A, \beta_A, \alpha_B, \beta_B} (\lambda_A \cdot |\mathbf{v}_A(\alpha_A, \beta_A) \circ \mathbf{n}| \\ & \quad + \lambda_B \cdot |\mathbf{v}_B(\alpha_B, \beta_B) \circ \mathbf{n}|) \quad (10) \end{aligned}$$

$$\text{s.t.} \begin{cases} \alpha_{A, \min} \leq \alpha_A \leq \alpha_{A, \max} \\ \beta_{A, \min} \leq \beta_A \leq \beta_{A, \max} \\ \alpha_{B, \min} \leq \alpha_B \leq \alpha_{B, \max} \\ \beta_{B, \min} \leq \beta_B \leq \beta_{B, \max} \\ \gamma_{A, B, \min} \leq \gamma \leq \gamma_{A, B, \max} \end{cases} \quad (11)$$

The factors λ_A and λ_B are constant weighting terms. The vectors \mathbf{v}_A and \mathbf{v}_B are normalized to length 1. To actually solve the constrained optimization problem, a sequential quadratic programming (SQP) approach was used [14]. This involves transforming the problem as stated in Eqs. (10) and (11) into standard form. Unlike written above, SQP requires the objective function to be minimized. Hence, the negative objective function is minimized:

$$\begin{aligned} & \operatorname{argmin}_{\alpha_A, \beta_A, \alpha_B, \beta_B} \{-\lambda_A \cdot |\mathbf{v}_A(\alpha_A, \beta_A) \circ \mathbf{n}| \\ & \quad + \lambda_B \cdot |\mathbf{v}_B(\alpha_B, \beta_B) \circ \mathbf{n}|\} \quad (12) \end{aligned}$$

Table 2 Constraints for A-plane geometry.

| Constraint set | $\alpha_{A, \min}$ | $\alpha_{A, \max}$ | $\beta_{A, \min}$ | $\beta_{A, \max}$ | λ_A |
|----------------|--------------------|--------------------|-------------------|-------------------|-------------|
| Opt1 | -90 | 0 | -10 | 10 | 1 |
| Opt2 | -90 | 0 | 0 | 0 | 1 |
| Opt3 | -90 | 0 | -10 | 10 | 1 |
| Opt4 | -90 | 0 | -10 | 10 | 1 |
| Opt5 | -90 | 0 | -10 | 10 | 1 |
| Opt6 | -90 | 0 | 0 | 0 | 1 |
| Opt7 | -90 | 0 | -10 | 10 | 1 |
| Opt8 | -90 | 0 | 0 | 0 | 1 |

Table 3 Constraints for B-plane geometry.

| Constraint set | $\alpha_{B, \min}$ | $\alpha_{B, \max}$ | $\beta_{B, \min}$ | $\beta_{B, \max}$ | λ_B |
|----------------|--------------------|--------------------|-------------------|-------------------|-------------|
| Opt1 | 0 | 120 | -10 | 10 | 1 |
| Opt2 | 0 | 120 | 0 | 0 | 1 |
| Opt3 | 0 | 120 | -10 | 10 | -1 |
| Opt4 | 0 | 120 | -10 | 10 | 1 |
| Opt5 | 0 | 120 | -10 | 10 | 1 |
| Opt6 | 0 | 120 | 0 | 0 | 1 |
| Opt7 | 0 | 120 | -10 | 10 | 1 |
| Opt8 | 0 | 120 | 0 | 0 | 1 |

Table 4 Constraints for angle between A-plane and B-plane, and optimization domain. Estimation of C-arm angulations for each ablation site separately or combined for all ablation sites per dataset.

| Con- straint set | $\gamma_{A, B, \min}$ | $\gamma_{A, B, \max}$ | Optimization for | |
|------------------------|-----------------------|-----------------------|-----------------------------|---------------------------------|
| | | | individual ablation line | both ablation lines together |
| Opt1 | 60 | 120 | x | |
| Opt2 | 60 | 120 | x | |
| Opt3 | 60 | 120 | x | |
| Opt4 | 60 | 120 | | x |
| Opt5 | 90 | 90 | x | |
| Opt6 | 90 | 90 | x | |
| Opt7 | 90 | 90 | | x |
| Opt8 | 90 | 90 | | x |

$$\text{s.t.} \begin{cases} \alpha_A - \alpha_{A, \max} \leq 0 \\ -\alpha_A + \alpha_{A, \min} \leq 0 \\ \beta_A - \beta_{A, \max} \leq 0 \\ -\beta_A + \beta_{A, \min} \leq 0 \\ \alpha_B - \alpha_{B, \max} \leq 0 \\ -\alpha_B + \alpha_{B, \min} \leq 0 \\ \beta_B - \beta_{B, \max} \leq 0 \\ -\beta_B + \beta_{B, \min} \leq 0 \\ |\mathbf{v}_A \circ \mathbf{v}_B| - \cos(\gamma_{A, B, \max}) \leq 0 \\ -|\mathbf{v}_A \circ \mathbf{v}_B| + \cos(\gamma_{A, B, \min}) \leq 0 \end{cases} \quad (13)$$

Initialization was performed with the following biplane C-arm angulations: $\alpha_A = -45, \beta_A = 0, \alpha_B = 45$ and $\beta_B = 0$.

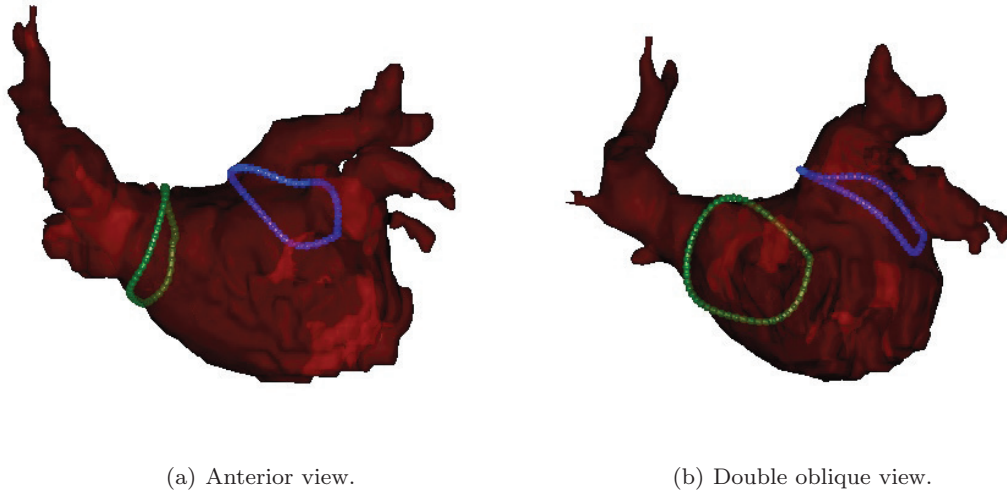


Fig. 2 Left atrium mesh model with ipsilateral ablation planning lines (dataset C5). The right sided planning line is colored green, the left sided blue, respectively. a) Anterior view under which the right sided planning line almost degenerates to a line under the chosen viewing direction. b) Double oblique viewing angle (49° LAO, 10° CAUD) onto the surface model. The right sided planning line (green) is seen far less foreshortened now, but the foreshortening of the blue ablation line has increased.

Table 5 Plane normal vectors for corresponding ablation lines and estimated optimal viewing angles for monoplane system and biplane system under constraints 'Opt1' and 'Opt2', respectively. In both cases, viewing directions are optimized to be as orthogonal as possible to the area of interest. For 'Opt2' no rotation in CRAN/CAUD direction was allowed. All values are in C-arm rotation angles.

| Case | Site | Plane normal | | Monoplane | | Opt1 | | | | | Opt2 | | | | |
|------|------|--------------|-----------|------------|-----------|------------|-----------|------------|-----------|----------------|------------|-----------|------------|-----------|----------------|
| | | α_A | β_A | α_A | β_A | α_A | β_A | α_B | β_B | $\gamma_{A,B}$ | α_A | β_A | α_B | β_B | $\gamma_{A,B}$ |
| C1 | RPV | -115.1 | 20.1 | 64.9 | -10.0 | -84.6 | 10.0 | 34.4 | -10.0 | 120.0 | -85.1 | 0.0 | 34.9 | 0.0 | 120.0 |
| C1 | LPV | 122.6 | 42.6 | -57.6 | -10.0 | -26.9 | -10.0 | 92.1 | 10.0 | 120.0 | -27.4 | 0.0 | 92.6 | 0.0 | 120.0 |
| C2 | RPV | -135.8 | 20.5 | 44.2 | -10.0 | 0.0 | -10.0 | 61.0 | -10.0 | 60.0 | 0.0 | 0.0 | 60.0 | 0.0 | 60.0 |
| C2 | LPV | 144.9 | 20.4 | -35.1 | -10.0 | -61.0 | -10.0 | 0.0 | -10.0 | 60.0 | -60.0 | 0.0 | 0.0 | 0.0 | 60.0 |
| C3 | RPV | -100.6 | 4.9 | 79.4 | -4.9 | -70.5 | 4.4 | 49.3 | -4.1 | 120.0 | -70.6 | 0.0 | 49.4 | 0.0 | 120.0 |
| C3 | LPV | 135.6 | 33.3 | -44.4 | -10.0 | -61.0 | -10.0 | 0.0 | -10.0 | 60.0 | -60.0 | 0.0 | -0.0 | 0.0 | 60.0 |
| C4 | RPV | -110.1 | 3.3 | 69.4 | -3.3 | -80.0 | 3.0 | 39.9 | -2.7 | 120.0 | -80.0 | 0.0 | 40.0 | 0.0 | 120.0 |
| C4 | LPV | 133.0 | 11.7 | -47.4 | -10.0 | -16.5 | -10.0 | 102.5 | 10.0 | 120.0 | -17.8 | 0.0 | 102.2 | 0.0 | 120.0 |
| C5 | RPV | -100.8 | 15.6 | 79.2 | -10.0 | -70.3 | 10.0 | 48.7 | -10.0 | 120.0 | -70.8 | 0.0 | 49.2 | 0.0 | 120.0 |
| C5 | LPV | 141.9 | 59.0 | -38.1 | -10.0 | -61.0 | -10.0 | 0.0 | -10.0 | 60.0 | -60.0 | 0.0 | 0.0 | 0.0 | 60.0 |
| C6 | RPV | -94.8 | 19.1 | 80.0 | -10.0 | -64.3 | 10.0 | 54.6 | -10.0 | 120.0 | -64.8 | 0.0 | 55.2 | 0.0 | 120.0 |
| C6 | LPV | 115.5 | 43.7 | -64.5 | -10.0 | -34.0 | -10.0 | 85.0 | 10.0 | 120.0 | -34.5 | 0.0 | 85.5 | 0.0 | 120.0 |
| C7 | RPV | -108.3 | 26.2 | 71.7 | -10.0 | -77.8 | 10.0 | 41.2 | -10.0 | 120.0 | -78.3 | 0.0 | 41.7 | 0.0 | 120.0 |
| C7 | LPV | 114.0 | 27.7 | -66.0 | -10.0 | -35.5 | -10.0 | 83.5 | 10.0 | 120.0 | -36.0 | 0.0 | 84.0 | 0.0 | 120.0 |
| C8 | RPV | -114.8 | -0.5 | 65.3 | 0.5 | -84.8 | -0.5 | 35.2 | 0.4 | 120.0 | -84.9 | 0.0 | 35.1 | 0.0 | 120.0 |
| C8 | LPV | 144.3 | 23.7 | -35.7 | -10.0 | -61.0 | -10.0 | 0.0 | -10.0 | 60.0 | -60.0 | 0.0 | 0.0 | 0.0 | 60.0 |
| C9 | RPV | -96.6 | 20.2 | 80.0 | -10.0 | -66.1 | 10.0 | 52.9 | -10.0 | 120.0 | -66.6 | 0.0 | 53.4 | 0.0 | 120.0 |
| C9 | LPV | 104.5 | 45.7 | -75.4 | -10.0 | -45.0 | -10.0 | 74.0 | 10.0 | 120.0 | -45.5 | 0.0 | 74.5 | 0.0 | 120.0 |
| C10 | RPV | -109.7 | 33.5 | 70.3 | -10.0 | -79.2 | 10.0 | 39.8 | -10.0 | 120.0 | -79.7 | 0.0 | 40.3 | 0.0 | 120.0 |
| C10 | LPV | 122.0 | 32.0 | -58.0 | -10.0 | -27.5 | -10.0 | 91.5 | 10.0 | 120.0 | -28.0 | 0.0 | 92.0 | 0.0 | 120.0 |

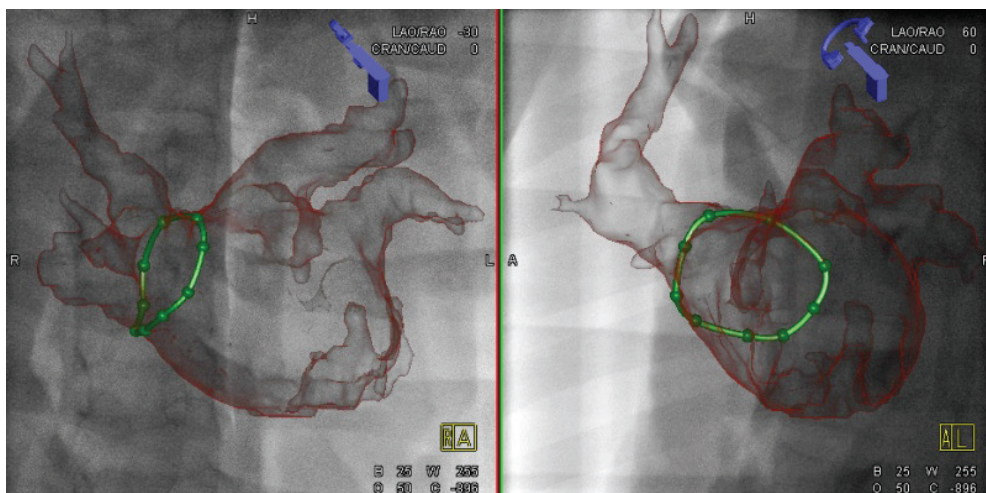
3 Evaluation

To evaluate our approach, the method was applied to 35 clinical datasets. Each dataset comprised a 3-D mesh model of the left atrium, segmented from a 3-D MRI image, as well as ablation planning lines associated with the mesh. All of the patients provided their informed consent for the analysis of their clinical data. The 3-D models were obtained using *syngo* InSpace EP (Siemens Healthcare, Forchheim, Germany). Wide-area circum-

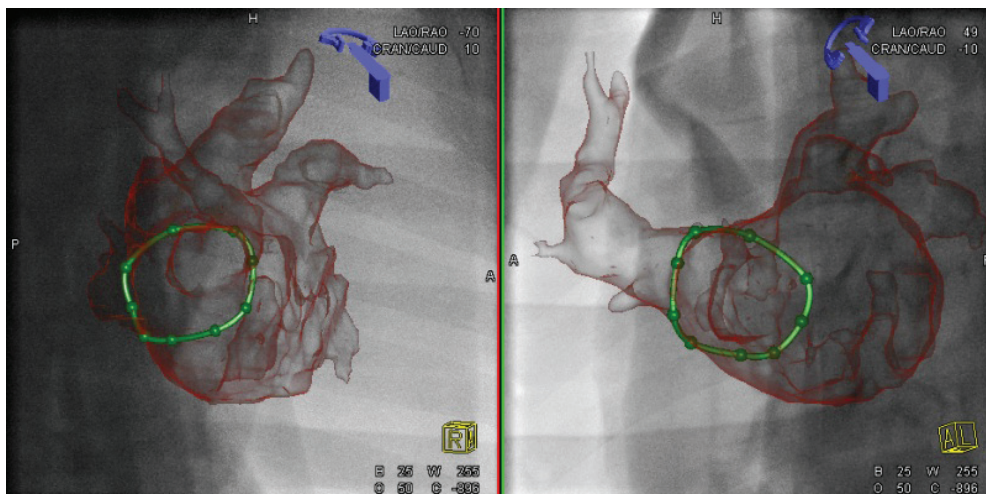
ferential ablation (WACA) lines were planned around the pulmonary vein ostia to guide ipsilateral pulmonary vein isolation. An example dataset with right- and left-sided ablation planning lines is shown in Figure 2.

3.1 Optimization Constraints

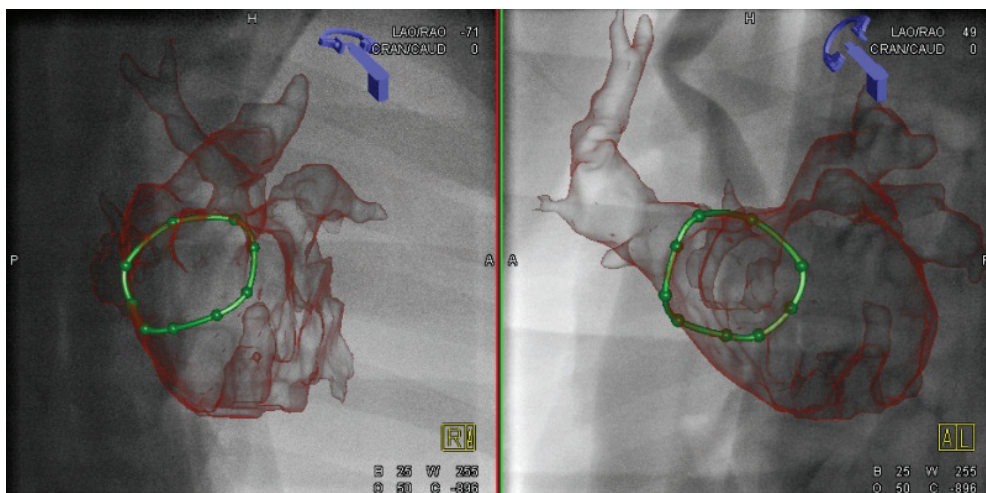
To study different use cases for our target application, atrial fibrillation treatment by PV isolation, different



(a) Std1



(b) Opt1



(c) Opt2

Fig. 3 Fluoro overlay image of dataset C5 as seen under different C-arm angulations. The contour of the 3-D surface model with right sided planning line is shown according to the chosen C-arm angulation. On the left in each image, we see the A-plane C-arm view, while the B-plane C-arm view is shown on the right. a) C-arm angulation according to standard view 'Std1'. b) Estimated optimal view under constraint set 'Opt1' ($\alpha_A = -70$, $\beta_A = 10$, $\alpha_B = 49$, $\beta_B = -10$). c) Estimated optimal view under constraint set 'Opt2' ($\alpha_A = -71$, $\beta_A = 0$, $\alpha_B = 49$, $\beta_B = 0$).

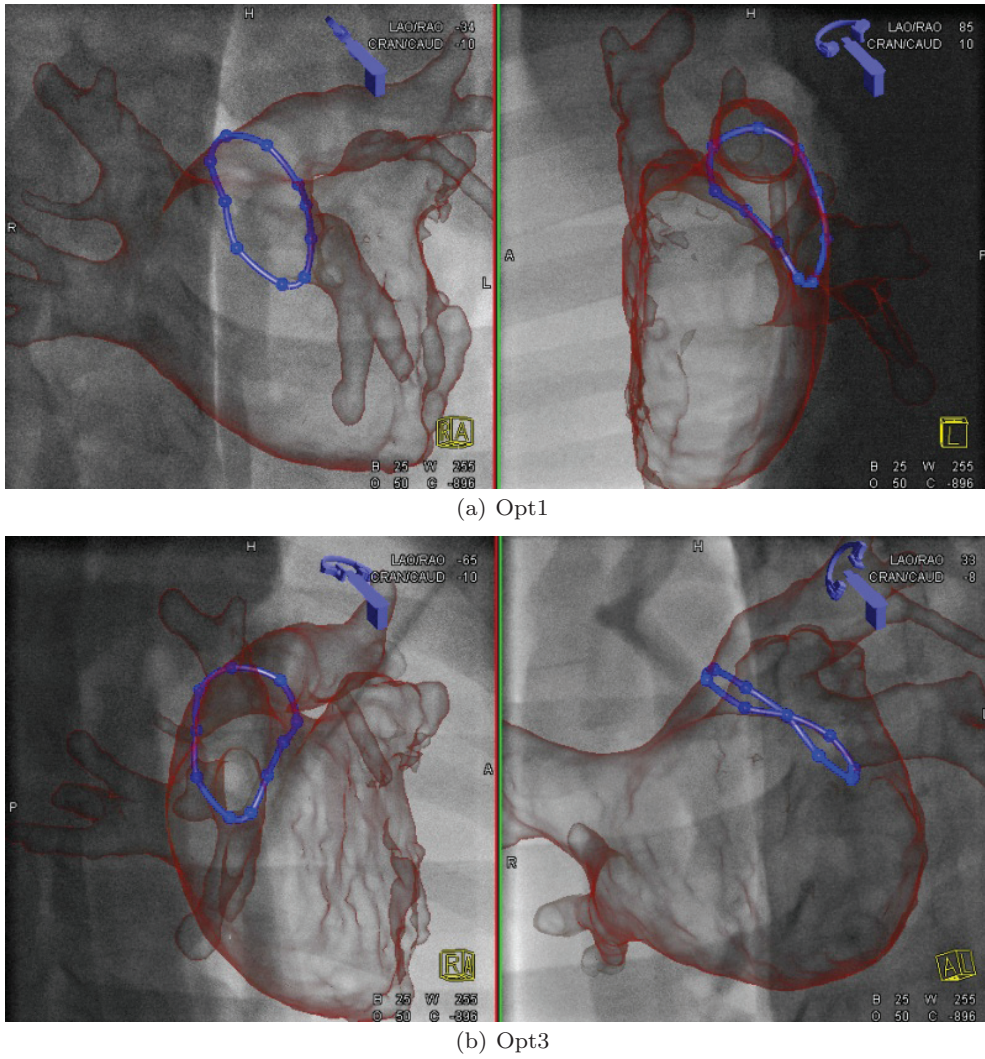


Fig. 4 Fluoro overlay image of dataset C6 as seen under different C-arm angulations. The left sided planning line is shown. The corresponding angulations are listed in Table 5 and Table 6. a) Estimated optimal view under constraint set 'Opt1' (LPV). b) Estimated optimal view under constraint set 'Opt3' (LPV).

optimization constraints were applied. For the first set of constraints, labeled 'Opt1', both C-arm viewing directions were optimized such that both have a mostly frontal view on the plane of interest. This was obtained by setting $\lambda_A = \lambda_B = 1$. The applicable domain for the C-arm rotation angles was set to $\alpha_A \in [-90, 0]$, $\beta_A \in [-10, 10]$, $\alpha_B \in [0, 120]$ and $\beta_B \in [-10, 10]$. The angle between the viewing directions of both C-arms was constraint to $\gamma_{A,B} \in [60, 120]$. The chosen angular domains also ensure that we always obtain one LAO and one RAO viewing direction. This set of constraints incorporates mechanical limitations of the C-arm gantry as well as application-specific constraints. In fact, many EP physicians prefer to limit the secondary angle to zero degrees to keep good patient access and to retain the possibility of moving the detector as close to the

patient as possible. This is reflected in constraint set 'Opt2'. 'Opt2' has the same constraints as 'Opt1' except that the secondary angles are limited to zero degree: $\beta_A = 0$, $\beta_B = 0$.

The configuration labeled 'Opt3' optimizes the C-arm viewing directions such that one imaging plane shows a frontal view on the ablation planning line, whereas the other imaging plane shows a sagittal view on the planning line. In the sagittal case, the ablation line, approximately an ellipse, may degenerate to (almost) a single line. The assignment of frontal and sagittal view to the imaging planes A and B is dynamic, i.e., either the A-plane or the B-plane may be used to obtain a frontal or a sagittal view, respectively. Both options were evaluated, and the configuration with the higher quality metric was chosen. The optimization goal of

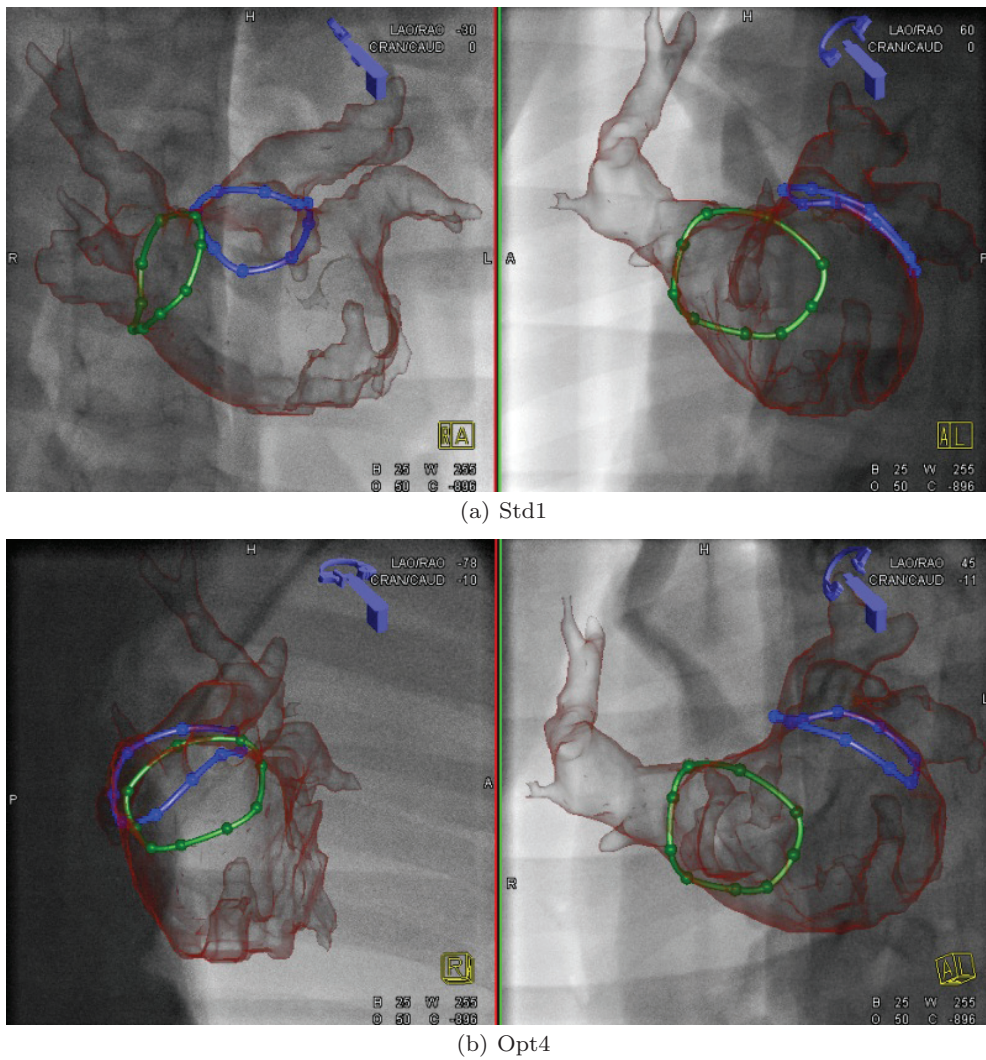


Fig. 5 Fluoro overlay image of dataset C5 as seen under different C-arm angulations. Right and left sided planning lines are shown. The corresponding angulations are listed in Table 7. a) C-arm angulation according to standard view 'Std1' (both PVs). b) Estimated optimal view under constraint set 'Opt4' (both PVs). Since one side is treated at a time during an actual ablation case, the other planned ablation line can be hidden. This way overlap of graphical objects can be avoided.

'Opt3' is reflected by the weights $\lambda_A = 1$ and $\lambda_B = -1$ in the objective function Eq. (10). The domain for the C-arm rotation angles is identical to 'Opt1'. C-arm view configurations obtained by using 'Opt3' could, e.g., be applied to cryoballoon (or other single-shot) ablation procedures to verify correct device placement [16]. Further details are discussed in Section 5. Constraint set 'Opt4' is conceptually similar to 'Opt1', however, optimal viewing angles are optimized for both ablation planning lines, right- and left-sided, at the same time. This is why only one set of optimal viewing angles is estimated, which will provide the best possible views on both planned ablation lines.

In addition to 'Opt1' to 'Opt4', we also wanted to investigate which optimized view configurations are possible for a fixed angle $\gamma_{A,B} = 90^\circ$. 'Opt5' and 'Opt6'

allowed for independent optimization based on right- and left-sided planning lines (either with or without secondary angle). In addition, 'Opt7' and 'Opt8' estimated C-arm angulations per case, similar to 'Opt4' (again either with or without secondary angle). A summary of all constraint parameters can be seen in Tables 2, 3 and 4 for A-plane, B-plane, and combined constraints, respectively. To simulate a monoplane system comprising only an A-plane, we employed the following angular constraints, $\alpha_A \in [-80, 80]$, $\beta_A \in [-10, 10]$. These sets comprise commonly used angulations for monoplane systems.

Table 6 Optimized viewing angles for biplane systems as obtained for 'Opt3' constraints. Unlike in the previous settings, the viewing directions are optimized to provide one (mostly) frontal view and one (approximately) sagittal view on the planning structure for the given optimization constraints. All angles are in degrees.

| | | Mono-plane | Opt3 | | | | |
|------|------|------------|------------|-----------|------------|-----------|----------------|
| Case | Site | α_A | α_A | β_A | α_B | β_B | $\gamma_{A,B}$ |
| C1 | RPV | 64.9 | -27.6 | -6.8 | 64.9 | -10.0 | 91.3 |
| C1 | LPV | -57.6 | -57.4 | -10.0 | 38.4 | -6.2 | 94.6 |
| C2 | RPV | 44.2 | -45.6 | 0.2 | 44.7 | -10.0 | 90.3 |
| C2 | LPV | -35.1 | -35.9 | -10.0 | 53.0 | 3.0 | 89.4 |
| C3 | RPV | 79.4 | -10.9 | -3.7 | 79.4 | -4.9 | 90.0 |
| C3 | LPV | -44.4 | -44.8 | -10.0 | 45.4 | 0.3 | 90.3 |
| C4 | RPV | 69.4 | -20.2 | -1.6 | 69.9 | -3.4 | 90.0 |
| C4 | LPV | -47.4 | -47.8 | -10.0 | 42.3 | -0.5 | 90.0 |
| C5 | RPV | 79.2 | -13.2 | -8.8 | 79.2 | -10.0 | 90.9 |
| C5 | LPV | -38.1 | -38.1 | -10.0 | 46.8 | 3.0 | 85.6 |
| C6 | RPV | 80.0 | -7.6 | -8.0 | 85.2 | -10.0 | 91.3 |
| C6 | LPV | -64.5 | -64.5 | -10.0 | 33.1 | -7.8 | 96.0 |
| C7 | RPV | 71.7 | -21.1 | -5.8 | 71.7 | -10.0 | 91.8 |
| C7 | LPV | -66.0 | -66.0 | -10.0 | 28.8 | -9.1 | 93.1 |
| C8 | RPV | 65.3 | -24.7 | 0.2 | 65.3 | 0.5 | 90.0 |
| C8 | LPV | -35.7 | -34.2 | -10.0 | 54.0 | 4.1 | 88.9 |
| C9 | RPV | 80.0 | -9.4 | -7.6 | 83.4 | -10.0 | 91.4 |
| C9 | LPV | -75.4 | -75.4 | -10.0 | 9.5 | 4.9 | 85.8 |
| C10 | RPV | 70.3 | -22.7 | -4.4 | 70.3 | -10.0 | 92.1 |
| C10 | LPV | -58.0 | -57.8 | -10.0 | 36.0 | -5.9 | 92.7 |

Table 7 Optimized viewing angles for biplane systems as obtained for 'Opt4' constraint. In this case one angulation was estimated. As a consequence, only one optimized view on both planning structures (RPV, LPV) is available. All angles are in degrees.

| Case | Monoplane RPV | | Monoplane LPV | | Opt4 | | | | |
|------|---------------|-----------|---------------|-----------|------------|-----------|------------|-----------|----------------|
| | α_A | β_A | α_A | β_A | α_A | β_A | α_B | β_B | $\gamma_{A,B}$ |
| C1 | 64.9 | -10.0 | -57.6 | -10.0 | -59.5 | -10.0 | 59.4 | 10.0 | 120.0 |
| C2 | 44.2 | -10.0 | -35.1 | -10.0 | -26.0 | -10.0 | 35.0 | -10.0 | 60.0 |
| C3 | 79.4 | -4.9 | -44.4 | -10.0 | -75.2 | -10.0 | 26.8 | -10.0 | 99.8 |
| C4 | 69.4 | -3.3 | -47.4 | -10.0 | -49.0 | -4.2 | 70.8 | 4.5 | 120.0 |
| C5 | 79.2 | -10.0 | -38.1 | -10.0 | -78.4 | -10.0 | 44.8 | -10.0 | 120.0 |
| C6 | 80.0 | -10.0 | -64.5 | -10.0 | -51.2 | -10.0 | 67.8 | 10.0 | 120.0 |
| C7 | 71.7 | -10.0 | -66.0 | -10.0 | -57.3 | -0.7 | 62.7 | 0.7 | 120.0 |
| C8 | 65.3 | 0.5 | -35.7 | -10.0 | -77.4 | -10.0 | 17.8 | -10.0 | 93.2 |
| C9 | 80.0 | -10.0 | -75.4 | -10.0 | -57.2 | -10.0 | 61.8 | 10.0 | 120.0 |
| C10 | 70.3 | -10.0 | -58.0 | -10.0 | -53.6 | 0.7 | 66.4 | -0.7 | 120.0 |

3.2 Quality Metric

To compare different viewing directions of a C-arm system for a planned ablation line, an objective quality metric is needed. As described before, planned ablation lines should appear with minimal foreshortening in the fluoroscopic projection images. Examples for projections from different viewing angles are shown in Figure 3 through Figure 5. Since the catheter has to be repositioned along the planned ablation line and contiguous ablation points have to be placed during a radiofrequency catheter ablation procedure, a maximal extent of the planning path in the projection image should make it easier to approach each ablation point as distinctly and accurately as possible. Otherwise, i.e., in case of foreshortening or overlap of certain parts of

the same ablation line, it may be difficult to clearly distinguish between neighboring ablation targets. As a consequence, we decided to use the overall length (circumference) of the ablation path as seen in the projection image as quality metric. For easier comparison, the length of the projected closed curve is normalized to the scale of 0 to 1. The lower bound corresponds to the minimal possible length and the upper bound to the maximal possible length, respectively. Both limits are determined per ablation line. A schematic drawing of minimal and maximal circumference of an ellipse projection is shown in Figure 6. The length of the ablation line as seen under X-ray is minimal for a sagittal view when the viewing direction is collinear to the major axis of the ellipse. The maximal length occurs when

Table 8 Optimized viewing angles for biplane systems under constraints 'Opt5' and 'Opt6'. The angle between both viewing directions $\gamma_{A,B}$ is fixed to 90° in these cases. All angles are in degrees.

| Case | Site | Monoplane | | Opt5 | | | | | Opt6 | | | | |
|------|------|------------|-----------|------------|-----------|------------|-----------|----------------|------------|-----------|------------|-----------|----------------|
| | | α_A | β_A | α_A | β_A | α_B | β_B | $\gamma_{A,B}$ | α_A | β_A | α_B | β_B | $\gamma_{A,B}$ |
| C1 | RPV | 64.9 | -10.0 | -69.2 | 10.0 | 19.0 | -10.0 | 90.0 | -70.1 | 0.0 | 19.9 | 0.0 | 90.0 |
| C1 | LPV | -57.6 | -10.0 | -11.7 | -10.0 | 76.5 | 10.0 | 90.0 | -12.4 | 0.0 | 77.6 | 0.0 | 90.0 |
| C2 | RPV | 44.2 | -10.0 | -1.6 | -10.0 | 90.2 | -10.0 | 90.0 | -0.8 | 0.0 | 89.2 | 0.0 | 90.0 |
| C2 | LPV | -35.1 | -10.0 | -81.0 | -10.0 | 10.8 | -10.0 | 90.0 | -80.1 | 0.0 | 9.9 | 0.0 | 90.0 |
| C3 | RPV | 79.4 | -4.9 | -55.5 | 3.6 | 34.3 | -3.3 | 90.0 | -55.6 | 0.0 | 34.4 | 0.0 | 90.0 |
| C3 | LPV | -44.4 | -10.0 | -90.0 | -10.0 | 1.8 | -10.0 | 90.0 | -89.4 | 0.0 | 0.6 | 0.0 | 90.0 |
| C4 | RPV | 69.4 | -3.3 | -65.0 | 2.4 | 24.9 | -2.3 | 90.0 | -65.1 | 0.0 | 24.9 | 0.0 | 90.0 |
| C4 | LPV | -47.4 | -10.0 | -1.5 | -8.2 | 87.3 | 8.2 | 90.0 | -2.0 | 0.0 | 88.0 | 0.0 | 90.0 |
| C5 | RPV | 79.2 | -10.0 | -54.9 | 10.0 | 33.3 | -10.0 | 90.0 | -55.8 | 0.0 | 34.2 | 0.0 | 90.0 |
| C5 | LPV | -38.1 | -10.0 | -84.0 | -10.0 | 7.8 | -10.0 | 90.0 | -83.1 | 0.0 | 6.9 | 0.0 | 90.0 |
| C6 | RPV | 80.0 | -10.0 | -49.0 | 10.0 | 39.3 | -10.0 | 90.0 | -49.8 | 0.0 | 40.2 | 0.0 | 90.0 |
| C6 | LPV | -64.5 | -10.0 | -18.6 | -10.0 | 69.6 | 10.0 | 90.0 | -19.5 | 0.0 | 70.5 | 0.0 | 90.0 |
| C7 | RPV | 71.7 | -10.0 | -62.4 | 10.0 | 25.8 | -10.0 | 90.0 | -63.3 | 0.0 | 26.7 | 0.0 | 90.0 |
| C7 | LPV | -66.0 | -10.0 | -20.1 | -10.0 | 68.1 | 10.0 | 90.0 | -21.0 | 0.0 | 69.0 | 0.0 | 90.0 |
| C8 | RPV | 65.3 | 0.5 | -69.8 | -0.4 | 20.2 | 0.4 | 90.0 | -69.7 | 0.0 | 20.3 | 0.0 | 90.0 |
| C8 | LPV | -35.7 | -10.0 | -80.1 | -10.0 | 11.7 | -10.0 | 90.0 | -80.7 | 0.0 | 9.3 | 0.0 | 90.0 |
| C9 | RPV | 80.0 | -10.0 | -50.7 | 10.0 | 37.5 | -10.0 | 90.0 | -51.9 | 0.0 | 38.1 | 0.0 | 90.0 |
| C9 | LPV | -75.4 | -10.0 | -29.6 | -10.0 | 58.6 | 10.0 | 90.0 | -30.5 | 0.0 | 59.5 | 0.0 | 90.0 |
| C10 | RPV | 70.3 | -10.0 | -63.9 | 10.0 | 24.3 | -10.0 | 90.0 | -64.7 | 0.0 | 25.3 | 0.0 | 90.0 |
| C10 | LPV | -58.0 | -10.0 | -11.9 | -10.0 | 76.3 | 10.0 | 90.0 | -12.8 | 0.0 | 77.2 | 0.0 | 90.0 |

Table 9 Optimized viewing angles for biplane systems under constraints 'Opt7' and 'Opt8'. Similar to 'Opt6' and 'Opt7', the angle between both viewing directions is fixed to 90° . However, only one angulation is estimated to provide an optimized view on both planning structures (RPV, LPV). All angles are in degrees.

| Case | Monoplane RPV | | Monoplane LPV | | Opt7 | | | | | Opt8 | | | | |
|------|---------------|-----------|---------------|-----------|------------|-----------|------------|-----------|----------------|------------|-----------|------------|-----------|----------------|
| | α_A | β_A | α_A | β_A | α_A | β_A | α_B | β_B | $\gamma_{A,B}$ | α_A | β_A | α_B | β_B | $\gamma_{A,B}$ |
| C1 | 64.9 | -10.0 | -57.6 | -10.0 | -44.3 | -9.0 | 44.2 | 9.0 | 90.0 | -45.1 | 0.0 | 44.9 | 0.0 | 90.0 |
| C2 | 44.2 | -10.0 | -35.1 | -10.0 | -41.8 | -10.0 | 50.0 | -10.0 | 90.0 | -40.5 | 0.0 | 49.5 | 0.0 | 90.0 |
| C3 | 79.4 | -4.9 | -44.4 | -10.0 | -71.6 | -10.0 | 20.2 | -10.0 | 90.0 | -71.0 | 0.0 | 19.0 | 0.0 | 90.0 |
| C4 | 69.4 | -3.3 | -47.4 | -10.0 | -34.2 | -3.3 | 55.6 | 3.6 | 90.0 | -33.9 | 0.0 | 56.1 | 0.0 | 90.0 |
| C5 | 79.2 | -10.0 | -38.1 | -10.0 | -65.9 | -10.0 | 25.9 | -10.0 | 90.0 | -65.2 | 0.0 | 24.8 | 0.0 | 90.0 |
| C6 | 80.0 | -10.0 | -64.5 | -10.0 | -36.1 | -8.4 | 52.5 | 9.5 | 90.0 | -36.7 | 0.0 | 53.3 | 0.0 | 90.0 |
| C7 | 71.7 | -10.0 | -66.0 | -10.0 | -42.3 | -0.5 | 47.7 | 0.5 | 90.0 | -42.3 | 0.0 | 47.7 | 0.0 | 90.0 |
| C8 | 65.3 | 0.5 | -35.7 | -10.0 | -75.1 | -10.0 | 16.6 | -10.0 | 90.0 | -75.0 | 0.0 | 15.0 | 0.0 | 90.0 |
| C9 | 80.0 | -10.0 | -75.4 | -10.0 | -41.9 | -9.0 | 46.6 | 9.4 | 90.0 | -42.8 | 0.0 | 47.2 | 0.0 | 90.0 |
| C10 | 70.3 | -10.0 | -58.0 | -10.0 | -38.6 | 0.4 | 51.4 | -0.4 | 90.0 | -38.6 | 0.0 | 51.4 | 0.0 | 90.0 |

the viewing direction is orthogonal to the plane defined by the major and minor axis of the ellipse.

3.3 Comparison to Standard Angulations

There are established standard C-arm view angles for electrophysiology ablation procedures. Common primary and secondary angles for A-plane and B-plane are listed in Table 1. Associated views were computed over all test data for each set of optimization criteria. The results are shown in Tables 11 and 12. The reported values serve as reference for our optimized C-arm viewing directions.

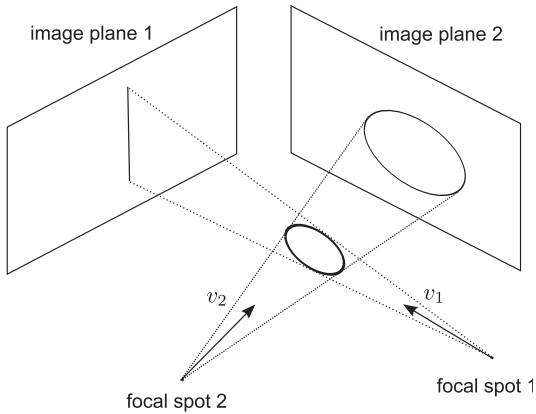
4 Results

The results of our evaluations are shown in Table 5 to Table 12. Table 5 through Table 9 lists estimated

optimal view angulations for constraint set 'Opt1' to 'Opt8', respectively. Only values for the first 10 datasets are listed. Due to mechanical C-arm system constraints, the plane normal vectors as well as the angulations for a monoplane system are not necessarily reachable. In Table 6 estimated angulations for 'Opt3' are presented along with monoplane angulations. Note that the angulation of the imaging plane representing the frontal view, which can either be the A-plane or the B-plane, is similar to the respective monoplane angulation. The slight differences found for some cases are due to the optimization constraints. Table 10 lists the overall estimated angles for each constraint set and imaging plane. The numbers reported in Table 11 and Table 12 represent the outcome of our quality metric. They were averaged over all evaluated datasets. For monoplane systems, only one C-arm viewing direction, the so-called A-plane view, is available. Since constraints due to the

Table 10 Average optimized viewing direction for C-arm system in degree (mean \pm std). Values are computed based on all 35 datasets.

| | Site | α_A | β_A | α_B | β_B | $\gamma_{A,B}$ |
|--------------|------|------------------|-----------------|-----------------|----------------|------------------|
| Plane normal | RPV | -108.3 ± 9.0 | 16.7 ± 8.9 | | | |
| Plane normal | LPV | 129.6 ± 12.0 | 37.9 ± 11.8 | | | |
| Monoplane | RPV | 71.1 ± 8.4 | -8.9 ± 2.6 | | | |
| Monoplane | LPV | -50.4 ± 12.0 | -10.0 ± 0.0 | | | |
| Opt1 | RPV | -74.7 ± 15.0 | 8.2 ± 4.2 | 42.8 ± 8.0 | -8.7 ± 2.8 | 118.3 ± 10.1 |
| Opt1 | LPV | -38.2 ± 17.9 | -10.0 ± 0.0 | 61.0 ± 44.9 | 3.1 ± 9.6 | 99.4 ± 28.9 |
| Opt2 | RPV | -75.1 ± 15.0 | 0.0 ± 0.0 | 43.2 ± 7.9 | 0.0 ± 0.0 | 118.3 ± 10.1 |
| Opt2 | LPV | -38.2 ± 17.2 | 0.0 ± 0.0 | 61.3 ± 45.2 | 0.0 ± 0.0 | 99.4 ± 28.9 |
| Opt3 | RPV | -20.1 ± 8.6 | -5.5 ± 2.9 | 71.7 ± 9.0 | -8.9 ± 2.6 | 90.8 ± 0.7 |
| Opt3 | LPV | -48.5 ± 13.9 | -9.4 ± 3.4 | 43.3 ± 14.9 | -1.1 ± 4.9 | 91.5 ± 4.5 |
| Opt4 | both | -60.9 ± 13.3 | -8.0 ± 3.2 | 52.1 ± 19.1 | 1.6 ± 8.9 | 112.8 ± 13.3 |
| Opt5 | RPV | -60.1 ± 12.8 | 7.9 ± 4.2 | 28.6 ± 13.2 | -8.4 ± 2.9 | 90.0 ± 0.0 |
| Opt5 | LPV | -35.9 ± 35.7 | -9.9 ± 0.3 | 53.5 ± 34.0 | 3.1 ± 9.6 | 90.0 ± 0.0 |
| Opt6 | RPV | -60.7 ± 13.0 | 0.0 ± 0.0 | 29.3 ± 13.0 | 0.0 ± 0.0 | 90.0 ± 0.0 |
| Opt6 | LPV | -36.2 ± 35.0 | 0.0 ± 0.0 | 53.8 ± 35.0 | 0.0 ± 0.0 | 90.0 ± 0.0 |
| Opt7 | both | -49.8 ± 16.1 | -7.5 ± 3.2 | 40.1 ± 15.2 | 1.1 ± 8.6 | 90.0 ± 0.0 |
| Opt8 | both | -49.9 ± 11.8 | 0.0 ± 0.0 | 40.1 ± 15.8 | 0.0 ± 0.0 | 90.0 ± 0.0 |

**Fig. 6** 2-D projection images of a 3-D ellipse from two different viewing directions. Viewing direction v_1 is collinear with the major axis of the ellipse. In this case, the length of the ellipse as seen under perspective projection is minimal. Viewing direction v_2 is orthogonal to major and minor axis of the ellipse. The circumference of the projected line is maximal.

B-plane C-arm system need not be taken into account, better view angles can be achieved. This is why we consider the results for the monoplane system as a benchmark to show what could be possible without the constraints due to a second imaging plane. The main benefit of a biplane C-arm system, beyond saving contrast agent during angiography examinations, is that 3-D information of the scene can be recovered by combining information from both planes [2].

For the constraint sets 'Opt1' and 'Opt2', the optimization yields similar results. On average, a scalar product of 0.81 could be achieved between the estimated and optimal viewing direction for constraint set 'Opt1', as reported in Table 11. The average scalar product for 'Opt2' was 0.74. The corresponding angles between the plane normal and the view orientation are

Table 11 Average scalar product of estimated viewing direction and optimal viewing direction. Values are computed based on all 35 datasets.

| | A-plane | B-plane | mean |
|-----------|-----------------|-----------------|-----------------|
| Monoplane | 0.92 ± 0.09 | | |
| Opt1 | 0.81 ± 0.07 | 0.80 ± 0.09 | 0.81 ± 0.08 |
| Opt2 | 0.75 ± 0.11 | 0.74 ± 0.12 | 0.74 ± 0.11 |
| Opt3 | 0.92 ± 0.09 | 0.0 ± 0.0 | 0.46 ± 0.05 |
| Opt4 | 0.70 ± 0.06 | 0.64 ± 0.08 | 0.67 ± 0.05 |
| Opt5 | 0.67 ± 0.05 | 0.67 ± 0.05 | 0.67 ± 0.05 |
| Opt6 | 0.61 ± 0.09 | 0.61 ± 0.09 | 0.61 ± 0.09 |
| Opt7 | 0.61 ± 0.10 | 0.56 ± 0.05 | 0.58 ± 0.06 |
| Opt8 | 0.59 ± 0.09 | 0.53 ± 0.06 | 0.56 ± 0.06 |
| Std1 | 0.46 ± 0.28 | 0.59 ± 0.34 | 0.52 ± 0.08 |
| Std2 | 0.59 ± 0.21 | 0.49 ± 0.36 | 0.54 ± 0.11 |
| Std3 | 0.39 ± 0.18 | 0.73 ± 0.18 | 0.56 ± 0.08 |

Table 12 Average relative length of projected ablation lines, scaled to $[0, 1]$ domain. Values are computed based on all 35 datasets.

| | A-plane | B-plane | mean |
|-----------|-----------------|-----------------|-----------------|
| Monoplane | 0.90 ± 0.12 | | |
| Opt1 | 0.82 ± 0.11 | 0.82 ± 0.09 | 0.82 ± 0.09 |
| Opt2 | 0.75 ± 0.16 | 0.74 ± 0.12 | 0.75 ± 0.13 |
| Opt3 | 0.90 ± 0.12 | 0.48 ± 0.16 | 0.69 ± 0.10 |
| Opt4 | 0.74 ± 0.08 | 0.74 ± 0.09 | 0.74 ± 0.07 |
| Opt5 | 0.72 ± 0.10 | 0.73 ± 0.09 | 0.72 ± 0.09 |
| Opt6 | 0.67 ± 0.14 | 0.66 ± 0.12 | 0.66 ± 0.11 |
| Opt7 | 0.68 ± 0.11 | 0.68 ± 0.10 | 0.68 ± 0.09 |
| Opt8 | 0.63 ± 0.12 | 0.67 ± 0.11 | 0.65 ± 0.09 |
| Std1 | 0.55 ± 0.20 | 0.74 ± 0.19 | 0.64 ± 0.11 |
| Std2 | 0.62 ± 0.16 | 0.69 ± 0.17 | 0.65 ± 0.11 |
| Std3 | 0.51 ± 0.19 | 0.78 ± 0.16 | 0.65 ± 0.11 |

35.9° and 42.3° , respectively. In the optimal case, when estimated and optimal viewing direction are collinear, the scalar product is 1. Fluoroscopy projection images with C-arm angulations estimated based on these con-

straint sets are shown in Figure 3, Figure 4 and Figure 5.

Which of the two C-arms to use when computing the frontal and sagittal views in 'Opt3' depended on the planning line under consideration. The goal was to always have one LAO view and one RAO view. Therefore, the analysis of evaluation results was performed per view, i.e., frontal and sagittal view, instead of A-plane and B-plane. For easier comparison with the other constraint sets in Table 11 and Table 12, the result for frontal view was listed under the A-plane column, and the result for the sagittal view was written into the B-plane column.

The average relative lengths of the ablation planning lines under optimized angulations are shown in Table 12. The numbers reported are scaled from 0 to 1, representing minimum and maximum possible length for the respective planning line, as explained above. The results are consistent with the ones reported in Table 11. The average maximum length of the projected ablation line is obtained in the monoplane case with 0.90 (for the A-plane). Comparing the results for 'Opt1' with the best standard view 'Std1' in more detail, we observed a maximal improvement of 69 % for the RPV of dataset C10. The relative length of the planning line increased from 0.45 to 0.76. The individual numbers are not listed for every dataset; however, the aggregated mean and standard deviation are reported in Table 12. Overall, the average relative length increased from 0.64 to 0.82, which reflects an improvement of about 28 %.

5 Discussion

We described a method for optimizing view directions based on ablation planning lines for AF procedures performed on interventional C-arm systems. We put special focus on biplane systems and accounted for their mechanical constraints, i.e., mechanically feasible rotation angles as well as the minimum angular separation between both C-arms. Furthermore, we evaluated different optimization strategies to meet the needs of different clinical applications. We benchmarked individually estimated view directions against commonly used standard angulations. Comparing the results for constraint set 'Opt1' and 'Opt2' nicely shows the benefit of permitting additional rotation in CRAN/CAUD direction. For both constraint sets, the range of feasible primary angles was identical (LAO/RAO). The only difference was in the domain of secondary rotation angles, which was limited to zero degrees for 'Opt2'. Comparing the optimized rotation angles for 'Opt1' and 'Opt2', as presented in Table 5, we see that the primary angles

are almost identical in both cases. Preventing any rotation in CRAN/CAUD direction impacts a view's performance metrics, i.e., the average scalar product and relative length of the projected planning lines suffer. This is why the optimization for 'Opt3' and 'Opt4' was performed including some secondary angle rotation, to achieve better results showing less foreshortening.

Constraint set 'Opt3', on the other hand, could be applied during procedures where a sagittal view on the structure of interest is important. This applies, e.g., to cryoballoon ablation procedures [19]. Table 6 reveals that one C-arm of the biplane system always moved into a frontal view. This can be seen by comparing the biplane views to the monoplane projection angle. The other C-arm of the biplane system moved to an almost perpendicular position, as shown by $\gamma_{A,B}$, providing the desired sagittal view. For cryoballoon procedures, a side view on the pulmonary vein ostia is needed to verify that the device was placed properly. This is further inspected by injecting contrast agent from the tip of the catheter into the pulmonary vein and confirming that there is a seal. No contrast must bypass the cryoballoon to ensure that a freeze can be obtained that leads to a durable circumferential lesion. Taking a closer look at the entries in Table 6, we notice that many of them somewhat resemble standard views as stated in Table 1.

The average length of the projected planned ablation lines onto the B-plane in 'Opt3' is rather high considering the low scalar product for this configuration. This is due to the chosen quality metric and the scaling involved. The length measurement was designed to provide good separation of different viewing angles close to an orthogonal view. However, in case of sagittal views, we look parallel onto an (almost) elliptical structure. This introduces ambiguities as ellipses have a major and minor axis. Dependent on the viewing direction being close to the major or minor axis, the length may differ considerably, even though both views are parallel to the structure. The relative length of 0 corresponds to a parallel view on the planning line along the major axis of the ellipse. Since our results were around 0.48, we conclude that most of our views were taken along the minor axis.

When working with 'Opt1' to 'Opt3', optimal viewing angles were calculated for each planning line separately. Such a strategy leads to two sets of angulations per case. In this case, the C-arms have to be moved from one position to another when treating the left PVs or the right PVs, respectively. In 'Opt4', on the other hand, only one set of optimized angles was calculated, providing a fixed view on both planning lines. As expected, results in terms of average scalar product and

length of projected ablation lines are lower compared to results for 'Opt1' and 'Opt2'. This reflects the trade-off between repositioning the C-arm for each ablation site in contrast to positioning it only once per case. However, the results for 'Opt4' are, on average, still better than the standard angulations 'Std1' to 'Std3'. This shows that adapting views to patients' anatomies outperforms the use of standard views in terms of foreshortening of planned ablation lines.

When optimizing view orientations under 'Opt5' to 'Opt8' the angle between both C-arms was fixed to 90° , as used by the standard angulations. The price to pay for introducing this additional constraint was less flexibility in view optimization as, e.g., expressed in lower quality metrics. Interestingly, the estimated average angles for A-plane and B-plane for these cases were about 60° RAO ($\alpha = -60$) and 30° LAO ($\alpha = 30$) for right-sided planning lines, and about (35° RAO, 55° LAO) for left-sided planning lines. Note that the second set of view angles is very close to the standard view directions (30° RAO, 60° LAO). If no further information about a patient's anatomy is taken into account, our results, therefore, suggest that one could use a (60° RAO, 30° LAO) view configuration when treating the RPVs and a (30° RAO, 60° LAO) setup when working on the LPVs, respectively. Put differently, instead of using only one fixed biplane C-arm view setup throughout the whole case, the C-arms should be repositioned from a configuration that is preferable for treating the left PVs into a second view setup that is more advantageous for ablating the right PVs. When one angulation was estimated for both planning lines, the average angles for A-plane and B-plane were about (50° RAO, 40° LAO), respectively. Interestingly, this is also close to the (45° RAO, 45° LAO) standard view configuration. This shows that the standard view angles are reasonable a priori choices. However, we also learned that they are not necessarily well adapted to individual patient anatomies. The large standard deviation especially for the LPV angulations confirms this.

Overall, the best values in terms of minimal foreshortening were achieved with 'Opt1' when estimating optimized views for right- and left-sided planning lines separately. The average angulations estimated for 'Opt1' for right-sided planning lines were about 75° RAO, 8° CRAN, and 43° LAO, 9° CAUD for A-plane and B-plane, respectively. For left-sided planning lines, the average estimated angulations were about 38° RAO, 10° CAUD, and 61° LAO, 3° CRAN for A-plane and B-plane, respectively.

Note that our proposed method is not limited to EP procedures. It could also be used for other applications such as closure of the left atrial appendage (LAA).

The placement of the Watchman device is carried out under fluoroscopy and transesophageal echocardiography [15]. If a 3-D model of the left atrium was available, then planning could be performed and be used to estimate optimal fluoroscopic views for the procedure. The PASS device release criterion could easily be verified in a sagittal view on the LAA ostium. This criterion states that the Watchman device has to be distal to or at the ostium of the LAA [10]. Another application is transcatheter aortic valve implantation (TAVI). During this procedure, an optimal sagittal fluoroscopic view is important for successful placement of the valve [8]. The targeted optimal view can be determined by three landmarks, the base of the aortic valve cusps, which form a triangle. In an optimal fluoroscopic view, these points lie on a plane perpendicular to the imaging plane [8].

6 Conclusions

We presented a method for estimating optimized view angulations for C-arm fluoroscopy system based on pre-procedural planning data. The method can accommodate individual constraints on the feasible projection angles for each fluoroscopy view individually as well as in relation to each other in case of biplane systems. Optimization for frontal or sagittal view directions is possible, depending on the application at hand. Our method was evaluated on clinical datasets, where planning lines were added to guide ipsilateral pulmonary vein isolation. Optimal C-arm angulations were computed for each ablation planning line and compared to standard angulations. Depending on the available degrees of freedom for optimizing the C-arm views and the patient anatomy, improvements of up to 69 % in terms of foreshortening of pre-planned ablation lines were found. On average, 28 % less foreshortening could be achieved when using constraint set 'Opt1' for the selection of biplane X-ray views. We also found that the standard view options provide very reasonable a priori choices. Their use is attractive, because physicians are already familiar with them. They should, however, be chosen judiciously depending on the selected treatment region and the therapy task at hand, e.g., using the method proposed in this paper.

Acknowledgements This work was supported by the German Federal Ministry of Education and Research (BMBF) in the context of the initiative Spitzencluster Medical Valley - Europäische Metropolregion Nürnberg, Project Grant Nos. 13EX1012A and 13EX1012E, respectively. Additional funding was provided by Siemens AG, Healthcare Sector. J. Hornegger gratefully acknowledge funding of the Erlangen Graduate School in Advanced Optical Technologies (SAOT) by the German Research Foundation (DFG) in the frame-

work of the German excellence initiative. We thank Dr. K. Kurzdin (Krankenhaus Barmherzige Brüder, Regensburg, Germany) for providing the clinical data. The concepts and information presented in this paper are based on research and are not commercially available.

Conflict of interest M. Koch and J. Hornegger have no conflict of interest. M. Hoffmann is funded by Siemens AG, Healthcare Sector, Forchheim, Germany. Norbert Strobel and Marcus Pfister are employees of Siemens AG, Healthcare Sector, Forchheim, Germany. The studies were carried out with support from Siemens AG, Healthcare Sector, Forchheim, Germany.

References

- Bourier, F., Vukajlovic, D., Brost, A., Hornegger, J., Strobel, N., Kurzdin, K.: Pulmonary vein isolation supported by MRI-derived 3D-augmented biplane fluoroscopy: A feasibility study and a quantitative analysis of the accuracy of the technique. *J. Cardiovasc. Electrophysiol.* **24**(2), 113–120 (2013)
- Brost, A., Strobel, N., Yatziv, L., Gilson, W., Meyer, B., Hornegger, J., Lewin, J., Wacker, F.: Geometric Accuracy of 3-D X-Ray Image-Based Localization from Two C-Arm Views. In: L. Joskowicz, P. Abolmaesumi, M. Fitzpatrick (eds.) *Workshop on Geometric Accuracy In Image Guided Interventions - Med Image Comput Comput Assist Interv (MICCAI)*, pp. 12–19 (2009)
- Chen, S., Carroll, J.: 3-d reconstruction of coronary arterial tree to optimize angiographic visualization. *IEEE Trans Med Imaging* **19**(4), 318–336 (2000)
- De Buck, S., Maes, F., Ector, J., Bogaert, J., Dymarkowski, S., Heidebuechel, H., Suetens, P.: An augmented reality system for patient-specific guidance of cardiac catheter ablation procedures. *IEEE Trans Med Imaging* **24**(11), 1512–1524 (2005)
- Dumay, A.C.M., Reiber, J., Gerbrands, J.J.: Determination of optimal angiographic viewing angles: basic principles and evaluation study. *IEEE Trans Med Imaging* **13**(1), 13–24 (1994)
- Garcia, J., Movassaghi, B., Casserly, I., Klein, A., James Chen, S.Y., Messenger, J., Hansgen, A., Wink, O., Groves, B., Carroll, J.: Determination of optimal viewing regions for x-ray coronary angiography based on a quantitative analysis of 3d reconstructed models. *Int J Cardiovasc Imaging* **25**(5), 455–462 (2009)
- Green, N.E., Chen, S.Y.J., Hansgen, A.R., Messenger, J.C., Groves, B.M., Carroll, J.D.: Angiographic views used for percutaneous coronary interventions: A three-dimensional analysis of physician-determined vs. computer-generated views. *Catheter Cardiovasc Interv* **64**(4), 451–459 (2005)
- Gurvitch, R., Wood, D.A., Leipsic, J., Tay, E., Johnson, M., Ye, J., Nietlispach, F., Wijesinghe, N., Cheung, A., Webb, J.G.: Multislice computed tomography for prediction of optimal angiographic deployment projections during transcatheter aortic valve implantation. *JACC Cardiovasc Interv* **3**(11), 1157–1165 (2010)
- Hassaguerre, M., Jas, P., Shah, D.C., Garrigue, S., Takahashi, A., Lavergne, T., Hocini, M., Peng, J.T., Roudaut, R., Clémenty, J.: Electrophysiological end point for catheter ablation of atrial fibrillation initiated from multiple pulmonary venous foci. *Circulation* **101**(12), 1409–1417 (2000)
- Kanmanthareddy, A., Reddy, Y.M., Pillarisetti, J., Swarup, V., Lakkireddy, D.: LAA closure with the watchman device. *Cardiac Interventions Today* **5**, 35–40 (2013)
- Keustermans, J., De Buck, S., Heidebuechel, H., Suetens, P.: Automated planning of ablation targets in atrial fibrillation treatment. In: *Proceedings of SPIE Medical Imaging*, vol. 7962, p. 796207 (2011)
- Kitslaar, P.H., Marquering, H.A., Jukema, W.J., Konig, G., Nieber, M., Vossepoel, A.M., Bax, J.J., Reiber, J.H.: Automated determination of optimal angiographic viewing angles for coronary artery bifurcations from CTA data. In: *Proceedings of SPIE Medical Imaging*, vol. 6918, p. 69181J (2008)
- Koch, M., Brost, A., Bourier, F., Hornegger, J., Strobel, N.: Automatic planning of atrial fibrillation ablation lines using landmark-constrained nonrigid registration. *Journal of Medical Imaging* **1**(1), 015,002 (2014)
- Nocedal, J., Wright, S.J.: *Numerical Optimization*, 2. edn. Springer Series in Operations Research. Springer, Berlin (2006)
- Perk, G., Biner, S., Kronzon, I., Saric, M., Chinitz, L., Thompson, K., Shiota, T., Hussani, A., Lang, R., Siegel, R., Kar, S.: Catheter-based left atrial appendage occlusion procedure: role of echocardiography. *Eur Heart J Cardiovasc Imaging* **13**(2), 132–138 (2012)
- Schmidt, B., Chun, K., Metzner, A., Ouyang, F., Kuck, K.H.: Balloon catheters for pulmonary vein isolation. *Herz Kardiovaskuläre Erkrankungen* **33**(8), 580–584 (2008)
- Tang, M., Gerds-Li, J.H., Nedios, S., Roser, M., Fleck, E., Kriatselis, C.: Optimal fluoroscopic projections for angiographic imaging of the pulmonary vein ostia: lessons learned from the intraprocedural reconstruction of the left atrium and pulmonary veins. *Europace* **12**(1), 37–44 (2010)
- Tung, R., Buch, E., Shivkumar, K.: Catheter ablation of atrial fibrillation. *Circulation* **126**(2), 223–229 (2012)
- Van Belle, Y., Janse, P., Rivero-Ayerza, M.J., Thornton, A.S., Jessurun, E.R., Theuns, D., Jordaens, L.: Pulmonary vein isolation using an occluding cryoballoon for circumferential ablation: feasibility, complications, and short-term outcome. *Eur. Heart J.* **28**(18), 2231–2237 (2007)